ROYAL SOCIETY
OF CHEMISTRY

PAPER

Check for updates

A new indoloquinoline-based fluorescence probe for imaging of hydrazine *in vitro* and *in vivo*

Caiju Zhang, [iD] †[a] Shi Tang,†[ab] Jianyong Wu,[a] Wenxing Lv, [iD] [c] Junjian Li*[b] and Chu Tang*[d]

The detection of hydrazine is critically important due to its potential to cause severe damage to ecosystems. Herein, a novel indoloquinoline-based "turn-off" fluorescent probe was specifically devised and fabricated for the detection of hydrazine. The probe demonstrates excellent qualities including rapid response, high sensitivity, excellent selectivity, and low cytotoxicity *in vitro*. Furthermore, this probe enables rapid imaging of hydrazine in living animals. These superior properties establish this probe as a promising tool for monitoring hydrazine levels *in vitro* and *in vivo*.
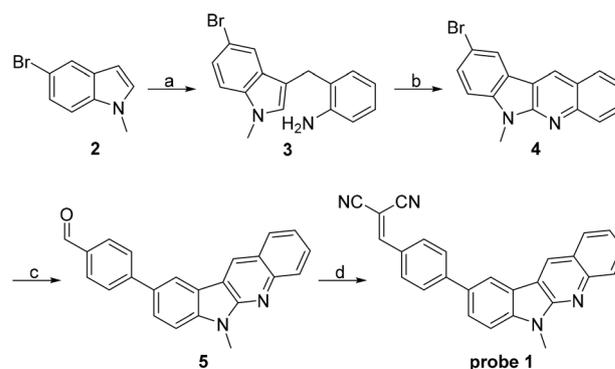
1. Introduction

Hydrazine (N_2H_4), a simple molecule first synthesized in 1875, plays a significant role in societal development.[1–3] However, its potential for pollution,[4] particularly through leakage during industrial production and use, poses serious threats to both ecosystems and human health.[5–7] This issue has raised considerable concern from the perspective of development. In response, many countries have stipulated allowable threshold values for hydrazine in water.[8,9] Consequently, there is a pressing need to develop novel methods for the specific, qualitative and quantitative detection of hydrazine.

The fluorescent detection approach has attracted considerable interest in analytical chemistry due to its promising properties for hydrazine detection, such as high sensitivity, good selectivity, and simple operation.[10–12] Since the first fluorescent probe for hydrazine detection was reported in 2006,[13] substantial progress has been made in this area, driven by the continuous efforts of scientists.[14,15] Most fluorescent probes are designed based on the strong nucleophilicity of hydrazine, which allows it to react with various recognition sites on the probes, resulting in either a "turn-on" or "turn-off" fluorescence response.[16–18] Among these recognition sites, the cyanovinyl group,[19] a strong electron-withdrawing moiety, is particularly noteworthy. It reacts with hydrazine to form a Schiff base,

making it an important component in hydrazine detection.[20–22] Recently, a variety of fluorophores, such as phenothiazine,[23,24] coumarin,[25,26] xanthene,[27] carbazole,[28] naphthalene,[29] and nopinone,[30] have been utilized to construct specific fluorescence probes incorporating cyanovinyl groups for detecting hydrazine.

The study of hydrazine detection applied in tumor imaging has been relatively limited.[31,32] Hydrazine, when absorbed and accumulated in tumor tissues due to drug metabolism, can exacerbate tumor progression by increasing drug resistance, promoting angiogenesis, and enhancing tumor aggressiveness through the synergistic enhancement of hypoxia.

Previously, we designed a probe that enables the detection of hydrazine (N_2H_4) in breast cancer tissues *via* targeting estrogen receptor α (ERα).[33] Herein, we report a novel near-infrared (NIR) fluorescent probe **1** (Scheme 1) that achieves N_2H_4 detection in breast cancer tissues without the need for a targeting moiety. Upon the addition of N_2H_4, the probe **1** exhibits a turn-off

[a]*Department of Radiology, Hainan Affiliated Hospital of Hainan Medical University (Hainan General Hospital), Haikou, 570311, P. R. China*

[b]*Key Laboratory of Tropical Biological Resources of Ministry of Education, School of Pharmaceutical Sciences, Hainan University, Haikou, 570228, P. R. China*

[c]*Hangzhou Institute of Advanced Technology Chinese Academy of Sciences, Hangzhou, 310024, P. R. China*

[d]*Engineering Research Center of Molecular and Neuro Imaging, Ministry of Education, School of Life Science and Technology, Xidian University, Xi'an, Shaanxi 710126, China. E-mail: ctang@xidian.edu.cn*

† These authors contributed equally to this work.

Scheme 1 Synthetic approach of probe **1**. Reaction settings: (a) 2-aminobenzyl alcohol, DCE, TFA, 50 °C, 12 h; (b) PIDA, HFIP, rt, 2 h; (c) 4-formylphenylboronic acid, Pd(PPh$_3$)$_4$, K$_2$CO$_3$, THF, 55 °C, 12 h; (d) malononitrile, piperidine, glacial acetic acid, EtOH, 85 °C, 12 h.

response. This occurs through the conversion of the electron-withdrawing cyanovinyl group into a hydrazone derivative, which disrupts the intramolecular charge transfer (ICT) process. Although various hydrazine-responsive probes have been designed for the detection of tumors, most of these probes have mainly been investigated at the cellular level, with relatively few studies focusing on *in vivo* tumor imaging (Table S1). In contrast, probe **1** exhibits a rapid turn-off response to N_2H_4 in MCF-7 breast cancer xenografts, demonstrating its potential for *in vivo* tumor imaging applications.

2.   Experimental section

2.1   Synthesis of probe 1

2.1.1   Synthesis of 2-((5-bromo-1-methyl-1*H*-indol-3-yl)methyl)aniline (3). A combination of (2-aminophenyl)methanol (1.17 g, 9.5 mmol), and 5-bromo-1-methyl-1*H*-indole (1.65 g, 7.9 mmol) in 40 mL of 1,2-dichloroethane was prepared in a nitrogen environment. Trifluoroacetic acid (0.27 g, 2.37 mmol) was introduced gradually into this mixture, and it was then subjected to heat in an oil bath (12 h) at 50 °C while being stirred. Reaction monitoring was carried out *via* thin-layer chromatography (TLC). When it was concluded, the mixture was neutralized *via* a Na_2CO_3 solution. Thereafter, it was subjected to extraction using CH_2Cl_2 three times. Following combining the organic layers, they were desiccated using anhydrous Na_2SO_4, filtrated, and then evaporated to obtain the product. Following this, it underwent purification through column chromatography to obtain **3** (1.488 g, 60% yield). ^{1}H NMR (400 MHz, CDCl$_3$) δ 7.72 (d, J = 1.8 Hz, 1H), 7.32 (dd, J = 8.7, 1.8 Hz, 1H), 7.17–7.2 (m, 3H), 6.81–6.68 (m, 1H), 6.72 (d, J = 7.7 Hz, 1H), 6.70 (s, 1H), 3.94 (s, 2H), 3.68 (s, 3H).

2.1.2   Synthesis of 9-bromo-6-methyl-6*H*-indolo[2,3-*b*]quinoline (4). To synthesize compound **4**, a solution of compound **1** (1.57 g, 5.0 mmol) in HFIP (40 mL) was prepared. To this solution, PIDA (1.93 g, 6.0 mmol) was added slowly at room temperature and the mixture was stirred for 2 h, with the reaction progress monitored by TLC. Upon completion of the reaction, water (20 mL) was added to the mixture, followed by extraction with ethyl acetate several times. After combining the organic layers, they were dried over anhydrous Na_2SO_4, filtered, and concentrated under reduced pressure. Finally, the resulting product underwent purification through column chromatography to afford **4** (1.038 g, 67% yield). ^{1}H NMR (400 MHz, CDCl$_3$) δ 8.70 (s, 1H), 8.27 (d, J = 2.0 Hz, 1H), 8.12 (d, J = 8.4 Hz, 1H), 8.02 (d, J = 8.0, 1H), 7.72–7.76 (m, 1H), 7.68 (dd, J = 8.4, 1.6 Hz, 1H), 7.46–7.50 (m, 1H), 7.31 (d, J = 8.8 Hz, 1H), 3.98 (s, 3H).

2.1.3   Synthesis of 4-(6-methyl-6*H*-indolo[2,3-*b*]quinolin-9-yl)benzaldehyde (5). Under a nitrogen environment, a mixture of **4** (0.31 g, 1 mmol), 4-formylphenylboronic acid (0.18 g, 1.2 mmol), K_2CO_3 (0.41 g, 3 mmol), and tetrakis(triphenylphosphine)palladium (10 mol%, 0.116 g) in THF (10 mL) was agitated at 55 °C for 12 h. The reaction was observed through TLC. Upon completion, the solvent was removed under reduced pressure. The residue underwent purification through column chromatography to afford **5** (0.2386 g, 71% yield). ^{1}H NMR (400 MHz, CDCl$_3$) δ 10.07 (s, 1H),

8.72 (s, 1H), 8.36 (d, J = 1.6 Hz, 1H), 8.16 (d, J = 8.4 Hz, 1H), 7.97–8.00 (m, 3H), 7.84–7.86 (m, 2H), 7.71–7.77 (m, 2H), 7.43–7.49 (m, 2H), 3.98 (s, 3H).

2.1.4   Synthesis of 2-(4-(6-methyl-6*H*-indolo[2,3-*b*]quinolin-9-yl)benzylidene)malononitrile (probe 1). Malononitrile (0.066 g, 1.0 mmol) and intermediate **5** (0.168 g, 0.5 mmol) were placed in a three-necked round-bottom flask (50 mL). The flask was purged with nitrogen. Subsequently, piperidine (1 mmol, 0.085 g), glacial acetic acid (0.090 g, 1.5 mmol), and ethanol (10 mL) were then added *via* syringe, followed by refluxing at 85 °C overnight in a nitrogen environment. After cooling to room temperature, the precipitated product was collected, washed three times with petroleum ether, and dried to afford probe **1** in 68% yield (130.6 mg). ^{1}H NMR (400 MHz, CDCl$_3$) δ 8.80 (s, 1H), 8.44 (d, J = 1.6 Hz, 1H), 8.17 (d, J = 8.4 Hz, 1H), 8.03–8.05 (m, 3H), 7.88–7.90 (m, 3H), 7.73–7.81 (m, 2H), 7.47–7.55 (m, 2H), 4.05 (s, 3H). ^{13}C NMR (100 MHz, CDCl$_3$) δ 159.32, 153.23, 147.93, 147.20, 143.51, 131.77, 130.96, 129.49, 129.38, 128.79, 128.06, 127.90, 127.79, 127.49, 124.40, 123.54, 121.44, 120.37, 118.02, 114.24, 113.16, 109.56, 81.45, 28.11. HRMS (ESI) *m/z*, computed for $C_{26}H_{16}N_4$, ([M + H]$^+$): 384.1375, obtained 385.1816.

2.2   Spectroscopic measurements

Probe **1** (1 mM) was first dissolved in DMSO, then diluted to a 10 μM stock solution with deionized water. The absorption and fluorescence spectra of probe **1** were measured before and after treatment with N_2H_4 (10 equiv.) for 5 min in a 37 °C water bath. For all fluorescence measurements, the excitation and emission slit widths were set to 5.0 nm.

2.2.1   Fluorescence titration. Various equivalents (0–3 equiv.) of N_2H_4 were added to a 10 μM solution of probe **1**. After incubation at room temperature for 5 min, the fluorescence spectra (λ_{ex} = 413 nm) were recorded. The detection limit (LOD) was measured following the previous method.[33]

2.2.2   Response time. To determine the response time of probe **1** towards N_2H_4, a solution of probe **1** (10 μM) was treated with N_2H_4 (1.5 equiv.) at 37 °C for different times. The fluorescence spectrum of the solution was measured immediately at the set time points (0–3 min).

2.2.3   Selectivity experiments. The competitive analytes and anions (10 mM) including N_2H_4, AcO^-, HPO_4^-, I^-, Br^-, Cl^-, Na^+, Ba^{2+}, Ca^{2+}, K^+, Zn^{2+}, Mn^{2+}, Cu^{2+}, Fe^{2+}, Pb^{2+}, HSO_3^-, Phe, Lys, Pro, Leu, Cys, Gly, Ile and Tyr were prepared using deionized water. Various analytes (10 equiv.) were added to the probe **1** (10 μM) solution and incubated at 37 °C for 2 min, after which the fluorescence spectra were recorded. Subsequently, N_2H_4 (1.5 equiv.) was added to the above mixture, and the fluorescence spectra were recorded again.

2.3   Cell culture

The human breast carcinoma cells MCF-7 (ATCC, USA), and normal breast epithelial cells MCF-10A (CCTCC, China), were cultured under controlled conditions. Both cell lines were maintained in DMEM supplemented with streptomycin (100 μg

mL^{-1}), penicillin (100 U mL^{-1}), and fetal bovine serum (10%) at 37 °C in a incubator with 5% CO_2.

2.4 *In vitro* biocompatibility

For assessing the biocompatibility of probe **1** with cells, an MTT assay was conducted. Initially, MCF-10A and MCF-7 cells were seeded into 96-well plates at a density of 8000 cells per well and allowed to adhere overnight. Thereafter, probe **1** with various concentrations (0, 2.5, 5, 10, 25, 50, 100 μM) was added into the wells, followed by incubating at 37 °C (72 h). Thereafter, MTT solution (20 μL, 5 mg mL^{-1}) was added into each well, and the plates were incubated for an additional 4 h. After removing the culture medium and washing the cells with PBS, DMSO (100 μL) was added to solubilize the formazan. Finally, absorbance at 590 nm was measured for all wells on a ELx808 Universal Microplate Reader.

2.5 Animal models

All animal procedures were performed in accordance with the Guidelines for Care and Use of Laboratory Animals of Hainan Medical University and approved by its Animal Ethics Committee. BALB/c nude female mice with mean age of 4–6 weeks were obtained from Chengdu Dossy Experimental Animals Co., Ltd and acclimatized for one week prior to experiments. To establish tumor xenografts, 100 μL of MCF-7 cell suspension (1 × 10^6 cells) were injected subcutaneously into the axillary area of the each mouse. When the mean tumor diameters reached approximately 5 mm, mice were used for *in vivo* imaging.

2.6 Fluorescence imaging (FLI)

After intratumoral injection of a hydrazine solution (20 μM), probe **1** (200 μL per mouse, 2.5 mg kg^{-1}, in PBS containing 5% DMSO) was administered intravenously *via* the tail vein. Fluorescence imaging was performed using a IVIS imaging system (PerkinElmer) with excitation and emission wavelengths established at 415 nm and 610 nm, respectively. Fluorescence images were acquired at appropriate time intervals (pre-injection, 0.5, 2, 4, 6, 8, 10, 12, and 24 h post-injection). The normal tissue-to-tumor ratio (NTTR) was calculated using regions of interest (ROIs) in both normal tissues and tumors as follows:

$$NTTR = \frac{\text{fluorescence intesity}_{\text{normal tissues}}}{\text{fluorescence intesity}_{\text{tumor}}}$$

3. Results and discussion

3.1 Synthesis

Scheme 1 displays the synthesis of probe **1**. Starting from 5-bromo-1-methyl-1*H*-indole (**2**), reaction with (2-aminophenyl)methanol afforded intermediate **3**. Subsequent cyclization–aromatization of **3** yielded intermediate **4**, which then underwent a Suzuki coupling reaction with 4-formylphenylboronic acid to give intermediate **5**. Finally, condensation of **5** with malononitrile in ethanol smoothly afforded the target probe **1**.

3.2 Sensitivity

To evaluate the optical response of probe **1** toward N_2H_4 detection, the absorption and emission of probe **1** in DMSO were analyzed with or without N_2H_4 using UV-Vis spectroscopy and fluorescence spectroscopy. As illustrated in Fig. 1a, probe **1** Initially displayed a strong absorption peak at 410 nm. On the other hand, after the addition of N_2H_4, this absorption peak was dramatically reduced followed by a noticeable color transition from yellow to colorless. For fluorescence spectroscopy, probe **1** demonstrated an intense red fluorescence emission at 615 nm (λ_{ex} = 413 nm, slit: 5 nm/5 nm) (Fig. 1b). This significant Stokes shift can be associated with the intramolecular charge transfer process. As N_2H_4 was incrementally added, the fluorescence intensity at 615 nm gradually reduced, eventually disappearing when the concentration of N_2H_4 reached 1.5 equivalent (Fig. 1c). The results in Fig. S1 further showed that within the concentration range of N_2H_4 from 0 to 1.2 equivalent, a direct correlation was observed between the fluorescent signal strength at 615 nm with the content of N_2H_4. This linearity is well-represented by the standard curve equation $Y = -3966.44x + 5078.73$, with a correlation coefficient (R^2) of 0.995. Theoretical calculations carried out based on the equation LOD = $3\delta/s$ (where δ is the standard deviation of the fluorescent signal strength and s represents the slope of the equation) determined the detection limit of probe **1** to be 0.68 μM. This low detection limit satisfies the requirements for detecting N_2H_4 concentrations in environmental and biological contexts. Finally, to investigate the reaction time between probe **1** and N_2H_4, the fluorescence properties of probe **1** were examined over a time span of 0 to 3 minutes following the reaction with N_2H_4. As shown in Fig. 1d, the fluorescence intensity at 615 nm was inversely correlated with the reaction time. A sharp decrease in fluorescence intensity was observed within 1 min following the addition of hydrazine and attained the lowest point at 2 min
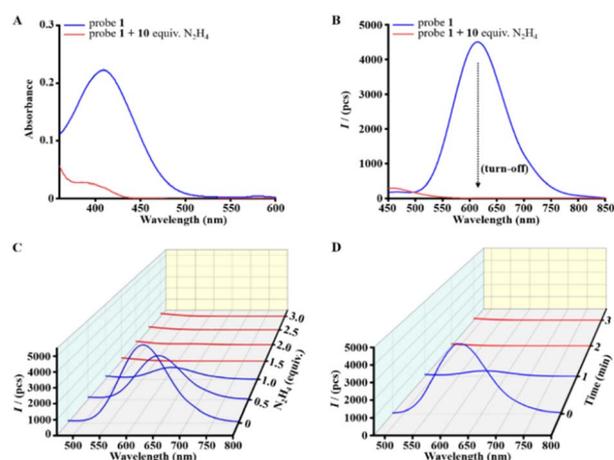

Fig. 1 Optical responsiveness of probe **1** (10 μM) to N_2H_4. Absorption (A) and fluorescence (B) spectra of probe **1** before and after adding hydrazine (10 equiv.). (C) Fluorescence spectra of probe **1** treated with various equivalent hydrazines. and (D) fluorescence turn-off response of probe **1** at 615 nm (λ_{ex} = 413 nm) upon adding hydrazine (1.5 equiv.) at various intervals.

and with no significant changes upon extending the reaction interval to 3 min. The results indicate that probe **1** is appropriate for the prompt determination of N₂H₄.

3.3 Selectivity

Fluorescence spectroscopy was used to assess the selectivity of probe **1** towards N₂H₄ in the presence of other substances. As depicted in Fig. 2, the addition of various substances (10 equiv., including AcO⁻, Cl⁻, Br⁻, I⁻, HPO₄⁻, Na⁺, Ba²⁺, Ca²⁺, K⁺, Zn²⁺, Mn²⁺, Cu²⁺, Fe²⁺, Pb²⁺, HSO₃⁻, Phe, Lys, Pro, Leu, Cys, Gly, Ile, and Tyr) did not alter the fluorescence intensity of probe **1** at 615 nm. Moreover, co-incubation of probe **1** with NH₃·H₂O (Fig. S2) or rat liver microsomes (Fig. S3) caused no significant change in its fluorescence intensity. In contrast, the introduction of N₂H₄ significantly quenched the fluorescence, indicating that the fluorescence output of probe **1** to N₂H₄ was specific. The findings confirm that probe **1** displays enhanced selectivity for N₂H₄ with negligible interference from other substances.

3.4 Study on the "turn-off" mechanism

To investigate this "turn-off" (*i.e.*, quenching) mechanism, high-resolution mass spectrometry (HRMS) of the reaction solution of probe **1** with N₂H₄ was conducted. The HRMS showed that the molecular ion peak of probe **1** ([M + H]⁺) at *m/z* was found at 385.1816 (Fig. S4), and the product **7** between N₂H₄ and probe 1 was found at *m/z* 351.1619 ([M + H]⁺) (Fig. S5). Besides, compound **7** was identified using ¹H NMR (Fig. S6) and ¹³C NMR spectra (Fig. S7). ¹H NMR (400 MHz, DMSO-*d₆*) δ 9.16 (s, 1H), 8.68 (d, *J* = 1.8 Hz, 1H), 8.14 (d, *J* = 7.7 Hz, 1H), 8.12 (d, *J* = 8.5 Hz, 1H), 7.96 (dd, *J* = 8.5, 1.6 Hz, 1H), 7.81–7.74 (m, 4H), 7.72 (d, *J* = 8.5 Hz, 1H), 7.63–7.61 (m, 2H), 7.53–7.50 (m, 1H), 6.83 (s, 2H), 3.96 (s, 3H). ¹³C NMR (100 MHz, DMSO-*d₆*) δ 152.9, 146.7, 142.4, 139.9, 138.5, 135.4, 132.4, 129.5, 129.3, 128.7, 127.6, 127.3, 127.1, 126.3, 124.3, 123.5, 120.8, 120.2, 118.2,
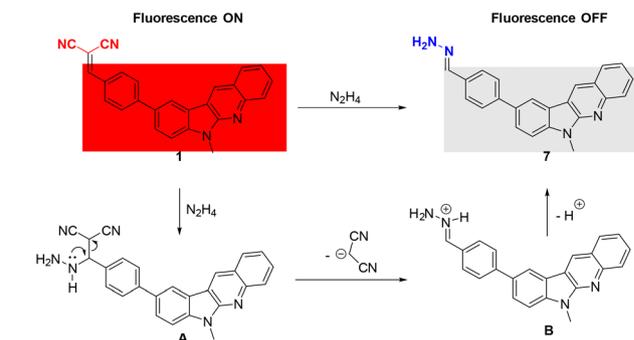
Scheme 2 The reaction mechanism of probe **1** with hydrazine.

110.2, 28.2. Based on these results and previous reports,[33–36] a plausible "turn-off" mechanism of probe **1** is proposed in Scheme 2. First, the electron-rich N₂H₄ attacked the malononitrile group of **1** to generate intermediate **A**. Following, the malononitrile anion left to deliver intermediate **B**. Finally, the deprotonation of intermediate **B** generated the hydrazone group.

3.5 *In vitro* biocompatibility

Before applying the probe **1** for the biomedical imaging, we investigated its biocompatibility in MCF-10A and MCF-7 cells. Cells viability was evaluated through MTT assay. At various concentrations, the probe **1** showed no obvious cytotoxicity to MCF-10A (Fig. 3A) and MCF-7 (Fig. 3B) cells after 72 h incubation, and both cell viability was higher than 77%. This indicated our probe was safe and nontoxic in cell level.

3.6 *In vivo* fluorescence imaging

Given the excellent *in vitro* sensing properties of probe **1** for hydrazine, we next investigated its potential application for imaging hydrazine in living animals. The MCF-7 tumor-bearing nude mice were intratumorally injected with hydrazine, followed by intravenous administration of probe **1** 10 min later. Real-time fluorescence images of each mouse were subsequently captured using the IVIS imaging system. As depicted in Fig. 4, probe **1** demonstrated a rapid response to hydrazine, as evidenced by the significant reduction in fluorescence signal in tumor tissues within 0.5 h post-injection, which remained
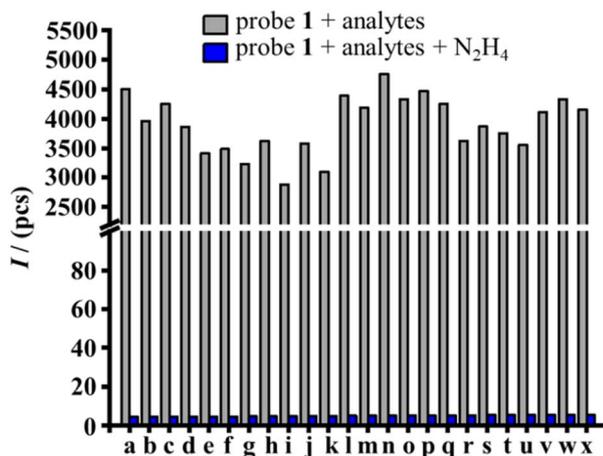

Fig. 2 The fluorescence intensity of probe **1** (10 μM) at 615 nm after treatment with varying analytes (10 equiv.) or analytes (10 equiv.) + N₂H₄ (1.5 equiv.). (a–x) None, AcO⁻, Cl⁻, Br⁻, I⁻, HPO₄⁻, Na⁺, Ba²⁺, Ca²⁺, K⁺, Zn²⁺, Mn²⁺, Cu²⁺, Fe²⁺, Pb²⁺, HSO₃⁻, Phe, Lys, Pro, Leu, Cys, Gly, Ile and Tyr.
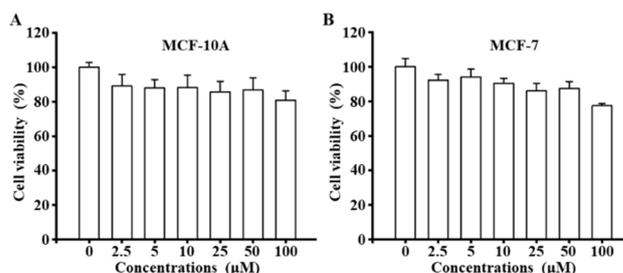

Fig. 3 *In vitro* biocompatibility evaluation of probe **1** after incubation with MCF–10A cells (A) and MCF–7 (B) cells.
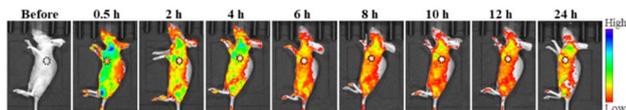
Fig. 4 Fluorescence imaging of probe **1** in MCF-7 tumor-bearing mice at various intervals pre- and post-injection.

undetectable at 24 h. Quantitative analysis showed that the NTTR values of probe **1** was 1.73 ± 0.45 at 0.5 h following administration as well as retained a high level (1.92 ± 0.52 at 12 h and 1.89 ± 0.42 at 24 h) post-injection (Fig. S8). These results demonstrate that the probe **1** has the potential to effectively detect hydrazine under physiological conditions.

4. Conclusion

In conclusion, a novel indoloquinoline-based "turn-off" fluorescence probe was developed hydrazine detection *via* the an ICT mechanism. This probe exhibits several outstanding qualities, including high sensitivity, rapid response, and excellent selectivity, and low cytotoxicity. Moreover, it has been successfully applied to image hydrazine in MCF-7 tumor-bearing nude mice. These attributes make it a promising tool for effectively monitoring hydrazine both *in vitro* and *in vivo*.

Conflicts of interest

The authors declare no competing financial interest.

Data availability

The data underlying this work are available in the published article and its supplementary information (SI). Supplementary information: comparison of hydrazine-detecting probes, linear relationship, fluorescence spectra, signal-to-background ratios, NMR, HRMS. See DOI: https://doi.org/10.1039/d5ra08919k.

Acknowledgements

References

1 A. Serov and C. Kwak, Direct hydrazine fuel cells: A review, *Appl. Catal. B Environ.*, 2010, **98**, 1–9.

2 I. C. Romão, S. M. C. Siqueira, F. O. M. D. Silva Abreu and H. S. D. Santos, Hydralazine and hydrazine derivatives: Properties, applications, and repositioning potential, *Chem. Biodivers.*, 2025, **22**, e202401561.

3 A. Dhenain, C. Darwich, C. M. Sabate, D. M. Le, A. J. Bougrine, H. Delalu, E. Lacote, L. Payen, J. Guitton, E. Labarthe and G. Jacob, (E)-1,1,4,4-Tetramethyl-2-tetrazene (TMTZ): A prospective alternative to hydrazines in rocket propulsion, *Chem. – Eur. J.*, 2017, **23**, 9897–9907.

4 B. B. Wang, M. Quinto, W. M. He, H. T. Qiu, X. L. Li and W. Zhao, Visual monitoring of hydrazine in food and environmental samples by wearable probe, *J. Hazard. Mater.*, 2024, **480**, 136384.

5 Y. Jung, I. G. Ju, Y. H. Choe, Y. Kim, S. Park, Y. M. Hyun, M. S. Oh and D. Kim, Hydrazine expose: The next-generation fluorescent probe, *ACS Sens.*, 2019, **4**, 441–449.

6 C. P. Cao, Q. Song, C. Y. H. Peng, S. X. Li, G. J. Mao, J. Ouyang, L. F. Hu, Y. F. Li and C. Y. Li, A fluorescent probe based solid-state fluorophore for the detection of N2H4 and its application in environmental samples, *J. Hazard. Mater.*, 2026, **501**, 140918.

7 J. Y. Ma, X. T. Kong, M. T. Zhao, Z. L. Jiao, X. S. Zhang, H. Xie and Z. X. Zhang, A water-soluble red-emitting fluorescence probe for detecting hazardous hydrazine in environmental waters and biosystems, *Sci. Total Environ.*, 2024, **944**, 173810.

8 L. Zhang and L. J. Cheng, Advances in optical probes for the detection of hydrazine in environmental and biological systems, *Crit. Rev. Anal. Chem.*, 2025, **55**, 53–82.

9 K. H. Nguyen, Y. Q. Hao, W. S. Chen, Y. T. Zhang, M. T. Xu, M. H. Yang and Y. N. Liu, Recent progress in the development of fluorescent probes for hydrazine, *Luminescence*, 2018, **33**, 816–836.

10 C. P. Ge, F. Pei, P. C. Zhang, X. Y. Wang, Z. Y. Li, Z. P. Sai, T. J. Ni, K. W. Chang and Z. J. Yang, Naked-eye and fluorescence resonance energy transfer based ratiometric fluorescent probe for rapid, sensitive and selective detection of hydrazine and its applications in imaging of environmental samples and living systems, *J. Hazard. Mater.*, 2025, **484**, 136781.

11 M. M. Xing, Y. Y. Han, Y. L. Zhu, Y. T. Sun, Y. Y. Shan, K. N. Wang, Q. X. Liu, B. L. Dong, D. X. Cao and W. Y. Lin, Two ratiometric fluorescent probes based on the hydroxyl coumarin chalcone unit with large fluorescent peak shift for the detection of hydrazine in living cells, *Anal. Chem.*, 2022, **94**, 12836–12844.

12 H. X. Tan, Z. L. Wang, X. Q. Yang, X. P. Rao, P. Zhao and Q. Jiang, Development of a ratiometric fluorescent probe based on caffeic acid for hydrazine detection and its applications in water samples and living cells, *Spectrochim. Acta, Part A Mol. Biomol. Spectrosc.*, 2025, **326**, 125191.

13 S. W. Thomas III and T. M. Swager, Trace hydrazine detection with fluorescent conjugated polymers: A turn-on sensory mechanism, *Adv. Mater.*, 2006, **18**, 107–1050.

14 X. J. Qin, M. J. Lin, Z. F. Lai, J. W. Mo, S. M. Wen and X. Y. Yang, the fluorescent and bioluminescent probes for detecting hydrazine in recent years, *Dyes Pigm.*, 2024, **231**, 112378.

15 A. Maiti, D. Banik, S. Halder, S. K. Manna, A. Karak, K. Jana and A. K. Mahapatra, Near-infrared fluorescent turn-on probe for hydrazine detection: environmental samples and live cell imaging, *Org. Biomol. Chem.*, 2023, **21**, 6046–6056.

16 A. Takagi, I. Takashima and K. Okuda, A turn-on fluorescent probe containing a β-ketoester moiety for the selective detection of intracellular hydrazine, *RSC Adv.*, 2025, **15**, 428–434.

17 Y. Jung, I. G. Ju, Y. H. Choe, Y. Ki, S. Park, Y. M. Hyun, M. S. Oh and D. Kim, Hydrazine exposé: The next-generation fluorescent probe, *ACS Sens.*, 2019, **4**, 441–449.

18 E. F. Wang, H. L. Ma, J. X. Lu, F. Y. Wang and J. Ren, Recent progress in the fluorescent probes for hydrazine detection, *Tetrahedron*, 2022, **124**, 132989.

19 Q. X. Li, Y. J. Yuan, R. X. Cheng, Y. Ma, R. Tan, Y. W. Wang and Y. Peng, An AIE-active tetra-aryl imidazole-derived chemodosimeter for turn-on recognition of hydrazine and its bioimaging in living cells, *Org. Biomol. Chem.*, 2024, **22**, 6135–6140.

20 M. J. Jung, S. J. Kim and M. H. Lee, π-Extended tetraphenylethylene containing a dicyanovinyl group as an ideal fluorescence turn-on and naked-eye color change probe for hydrazine detection, *ACS Omega*, 2020, **5**, 28369–28374.

21 L. X. Xiong, W. M. Li, Z. Y. Xie, B. Wang and G. D. Feng, A malononitrile-based portable fluorescent probe for ultrasensitive detection of hydrazine in environmental matrices, *Talanta*, 2026, **297**, 128607.

22 F. Xiao, J. H. Dong, R. C. Zhu, H. Bai, C. F. Zhao, B. Y. Zu, Y. C. Cui and Z. Z. Cai, Zero-fluorescence probe for ultrasensitive and specific detection of hydrazine by regulating the electron-accepting strength, *Anal. Chem.*, 2025, **97**, 8939–8946.

23 X. Y. Qiu, S. J. Liu, Y. Q. Hao, J. W. Sun and S. Chen, Phenothiazine-based fluorescence probe for ratiometric imaging of hydrazine in living cells with remarkable stokes shift, *Spectrochim. Acta, Part A Mol. Biomol. Spectrosc.*, 2020, **227**, 117675.

24 X. F. Sun, X. Jiang, Z. D. Wang, Y. Li, J. S. Ren, K. L. Zhong, X. P. Li, L. J. Tang and J. R. Li, Fluorescent probe for imaging N2H4 in plants, food, and living cells and for quantitative detection of N2H4 in soil and water using a smartphone, *J. Hazard. Mater.*, 2024, **479**, 135701.

25 L. Shan, X. W. Li, Z. Yu, X. L. Zheng, H. H. Ren, J. S. Wu, C. T. Lv, P. F. Wang and W. M. Liu, Coumarin bialdehyde-based fluorescent probe for the detection of hydrazine in living cells, soil samples and its application in test strips, *Spectrochim. Acta, Part A Mol. Biomol. Spectrosc.*, 2025, **343**, 126540.

26 W. J. Chang, W. Y. Yang, X. X. Wang, F. L. Xu, W. B. Zhang and J. H. Qian, Colorimetric and ratiometric fluorescent probes for sensitive visualization of hydrazine in water and in living cells, *Anal. Methods*, 2025, **17**, 8120–8126.

27 Y. B. Zhang, J. Hu, X. Q. Rong, J. Jiang, Y. Wang, X. T. Zhang, Z. H. Xu, K. Xu, M. Wu and M. X. Fang, Development of a hybrid rhodamine-hydrazine NIR fluorescent probe for sensitive detection and imaging of peroxynitrite in necrotizing enterocolitis model, *Bioorg. Chem.*, 2024, **152**, 107729.

28 R. M. Chen, B. K. Li, X. X. Qin, S. Xing, H. J. Ren, F. Ma, J. B. Chen and Q. F. Niu, A new carbazole based fluorescent probe with AIE characteristic for detecting and imaging hydrazine in living cells, mungbean sprouts, Arabidopsis thaliana, and practical samples, *Talanta*, 2024, **273**, 125953.

29 C. H. Zeng, Z. Y. Xu, C. Song, T. Y. Qin, T. H. Jia, C. Zhao, L. Wang, B. Liu and X. Peng, Naphthalene-based fluorescent probe for on-site detection of hydrazine in the environment, *J. Hazard. Mater.*, 2023, **445**, 130415.

30 S. Zhang, J. X. Tian, S. Gong, Z. Y. Meng, Y. Y. Liang, Y. Gu, M. R. Wang, Z. L. Wang and S. F Wang, A novel biphenyl tetrahydroindazole-type fluorescent probe for the detection of hydrazine and its applications in food detection, environmental analysis and biological imaging, *Spectrochim. Acta, Part A Mol. Biomol. Spectrosc.*, 2026, **347**, 126966.

31 B. Roy, S. Halder, A. Guha and S. Bandyopadhyay, Highly selective sub-ppm naked-eye detection of hydrazine with conjugated-1,3-diketo probes: Imaging hydrazine in drosophila larvae, *Anal. Chem.*, 2017, **89**, 10625–10636.

32 S. Nandi, A. Sahana, S. Mandal, A. Sengupta, A. Chatterjee, D. A. Safin, M. G. Babashkina, N. A. Tumanov, Y. Filinchuk and D. Das, Hydrazine selective dual signaling chemodosimetric probe in physiological conditions and its application in live cells, *Anal. Chim. Acta*, 2015, **893**, 84–90.

33 C. Tang, H. J. Tong, B. Liu, X. N. Wang, Y. S. Jin, E. L. Tian and F. Wang, Robust ERα-targeted near-infrared fluorescence probe for selective hydrazine imaging in breast cancer, *Anal. Chem.*, 2022, **94**, 14012–14020.

34 C. Y. Wu, R. H. Xie, X. Pang, Y. Q. Li, Z. L. Zhou and H. Li, A colorimetric and near-infrared ratiometric fluorescent probe for hydrazine detection and bioimaging, *Spectrochim. Acta, Part A Mol. Biomol. Spectrosc.*, 2020, **243**, 118764.

35 J. B. Qiu, Y. X. Cheng, S. J. Jiang, H. Y. Guo and F. F. Yang, A fluorescent sensor based on aggregation-induced emission: highly sensitive detection of hydrazine and its application in living cell imaging, *Analyst*, 2018, **143**, 4298–4305.

36 T. T. Zhang, Y. B. Lai and W. Y. Lin, Design of a ratiometric near-infrared fluorescent probe with double excitation for hydrazine detection *in vitro* and *in vivo*, *Sci. Total Environ.*, 2022, **837**, 155462.